IEEE Access
Multidisciplinary ⋮ Rapid Review ⋮ Open Access Journal

Received 7 August 2023, accepted 27 August 2023, date of publication 31 August 2023, date of current version 7 September 2023.

Digital Object Identifier 10.1109/ACCESS.2023.3310540

RESEARCH ARTICLE

Efficient Tuning Scheme of Mode-Switching-Based Powertrain Oscillation Controller Considering Nonlinear Backlash

HEISEI YONEZAWA, (Member, IEEE), ANSEI YONEZAWA, (Member, IEEE), AND ITSURO KAJIWARA

Division of Mechanical and Aerospace Engineering, Hokkaido University, Sapporo 060-8628, Japan

Corresponding author: Heisei Yonezawa (yonezawah@eng.hokudai.ac.jp)

This work was supported in part by the Japan Society for the Promotion of Science under Grants-in-Aid for Scientific Research Programs under Grant 22K20396 and Grant 23K13273, and in part by the Transmission Research Association for Mobility Innovation (TRAMI) under Grant 23B3-01.

ABSTRACT For enhancement of the drivability and lifetime of the components, reduction in vehicle driveline oscillations has been addressed by advanced active control algorithms. However, most of the existing works involve subjective determination of their critical controller parameters, imposing heavy adjustment tasks on designers. This research presents an efficient tuning algorithm of the model-based driveline vibration controller that explicitly considers the adverse influences due to nonlinear backlash. First, a driveline dynamics model with a dead-zone effect of backlash is established. A dynamic output feedback H_2 controller is designed as a baseline controller to attenuate the low-frequency resonance of a driveline. A simple control mode switching algorithm is combined with the controller to deal with the backlash nonlinearity. The optimal values of their important design parameters included in the active control system are automatically searched by a computationally efficient algorithm, i.e., the simultaneous perturbation stochastic approximation (SPSA). The proposed active oscillation controller tuned by the SPSA is validated via several simulation tests. The robustness is evaluated for various patterns of driveline dynamics fluctuations such as the model parameters, the length of backlash, and the driving conditions. Moreover, the proposed controller is compared to traditional active controllers including a proportional-integral-differential (PID) controller tuned by the Ziegler-Nichols method. As a result, the improvement of the vibration suppression performance as well as its robustness originating from the compensation for backlash is revealed.

INDEX TERMS Active vibration control, drivetrain, efficient optimization, nonlinear backlash, robustness evaluation, simultaneous perturbation stochastic approximation.

I. INTRODUCTION

With the recent trend toward downsizing, weight reduction, and high performance in mechanical and automotive systems, the importance of vibration suppression technology has become more pronounced [1], [2]. There are two basic categories of vibration suppression: passive control [3], [4] and active control [5], [6]. In particular, active vibration control has been widely investigated because of their high attenuation ability [7], [8].

Vibration suppression is also one of the indispensable key technologies for automotive powertrains [9], [10]. When an abrupt change occurs in a driving torque, transient vibrations are caused in an automotive driveline, significantly providing adverse influences for the comfortability and lifetime of the parts. Active vibration suppression has been known to be one of the powerful countermeasures because it allows for higher attenuation effects based on advanced control technologies. For example, a disturbance rejection approach with an

The associate editor coordinating the review of this manuscript and approving it for publication was Wei Liu.

adaptive disturbance observer (ADO) [11], an adaptive active control [12], and a model reference adaptive linear quadratic tracking (ALQT) controller have been implemented to effectively reduce vehicle oscillations [13]. Recently, the development of controllers with network communication-induced delay compensation has facilitated implementation in modern vehicles [14], [15].

The above control approaches neglect the nonlinear backlash, which results in the growth of the oscillation amplitude [16], [17], caused within a gear of driveline. The backlash makes a driveline mechanism discontinuously change between two dynamics: ''contact mode'' where the mechanical connection is established through the driveline and ''backlash mode'' where the motor and wheel sides are decoupled because of the clearance crossing. Such nonlinearity forces us to tackle a challenging situation with difficulty in the design of a more complicated active control structure [16], [17], [18], [19], [20], [21]. Specifically, advanced control schemes are required. Switching control strategies according to the two modes are promising [18], [19]. In [16] and [18], a clunk controller based on a soft landing reference governor was proposed to reduce the impact due to backlash. In [20], backlash was addressed in a flatness-based feedforward control logic. This was combined with a proportional feedback controller to actively damp driveline oscillations. Another study has used a control-oriented model and an extended state observer [21]. In [17], a control mode switching algorithm was applied to a model-based driveline oscillation controller. This algorithm is aimed at effectively reducing the shock after backlash traversal is finished.

Moreover, some driveline oscillation controllers considering backlash have been reported such as a robust disturbance observer-based approach [22] and applications of sliding mode control techniques [23], [24]. One of the most reasonable concepts is switching of the control strategies according to contact or backlash mode. Such examples include a linear-quadratic regulator (LQR) and a proportional-integral-differential (PID) controller [25].

Nevertheless, there remain issues in most of the conventional works:

- The above previous studies do not provide an efficient tuning scheme of multiple design parameters required for driveline oscillation control considering backlash. The automatic optimization process has the benefits of decreasing the designer's subjective tasks and improvement of the attenuation.
- A strategy to compensate for backlash needs to be simpler with fewer online calculation requirements.

As is generally known, the application of optimization algorithms efficiently generates the appropriate solution to feedback control problems [26], [27]. Some works have reported the idea that formulates powertrain dynamics controls as optimization problems [28]. Their applications include fuzzy logic-based gear shifting and engine operation controllers refined with an Interactive Adaptive-Weight Genetic Algorithm [29], [30]. Those papers have implied the importance of iterative offline simulations with powertrain models and the necessity of introducing efficient optimization algorithms.

Among active oscillation reduction techniques for a driveline, optimization problems introduced to compromise with some competing requirements can be found. For example, a model-based torque shaping controller was proposed to reduce the induced impact when a clunk occurs in backlash while enabling a smooth response during crossing in backlash [16]. Another study found that the genetic algorithm (GA) can give the optimal weighting coefficients required to design an LQR vibration controller [31]. Recently, the application of Bayesian optimization was reported to be useful [32]. Many works have employed a model predictive control (MPC)-based approach [33], [34], [35] because of its attractiveness of being able to determine optimal control commands online while explicitly handling limitations.

Nevertheless, there are still residual problems in the above existing studies, such as neglecting backlash nonlinearity, the absence of auto-tuning of important controller parameters (e.g., contact mode controller) by efficient optimization algorithms, and the necessity of online high computational tasks. Moreover, a simpler backlash compensation strategy is required to be combined with the optimization.

To tackle these issues, this paper presents an efficient tuning algorithm of a model-based driveline vibration controller considering the nonlinearity of backlash based on SPSA. This is an improved work of our previous studies [17], [36] in which the critical control parameters were subjectively set via the designer's trial-and-error adjustments. According to the contact and backlash modes, the backlash compensation is constructed to be a simple control mode switching algorithm combined with a single model-based H_2 controller. The proposed algorithm is aimed at sufficiently suppressing the low-frequency resonance of a driveline while alleviating the impact caused during the backlash mode. The critical control parameters, which are required for both the active damping and the backlash compensation, are automatically determined based on SPSA, focusing on its computational efficiency. SPSA [37], [38] is an optimization algorithm, which can be classified as the stochastic approximation method. The algorithm stochastically approximates the gradient of a loss function (objective function) to be minimized based on the simultaneous perturbation vector. Specifically, at each iteration, the gradient is stochastically estimated by providing simultaneous random perturbations for all design variables together. A remarkable advantage of SPSA is its superior computational efficiency. This is because loss function calculations are necessary to be performed only twice to estimate the gradient at each iteration, and it is independent of the dimension of optimization problems. Based on SPSA, this study designs the oscillation controller for the contact mode and the soft-landing compensator for the backlash mode. All the critical tuning parameters for the contact and backlash mode controls are stored in a vector updated by SPSA.

Therefore, both the contact and backlash mode controls can be optimized based on the simultaneous perturbation technique at once. The proposed scheme can automatically tune the driveline control system, leading to a decrease in adjustments depending on the designer's trial-and-error tasks.

The contributions of this paper are summarized below.

(C1). An efficient tuning scheme of an active H_2 oscillation controller with compensation for backlash is presented. In the present method, the simultaneous perturbation stochastic approximation (SPSA) automatically searches for the optimal controller parameters to decrease trial-and-error tasks imposed on designers. To the best of our knowledge, this work shows the first application of SPSA for driveline active oscillation suppression.

(C2). The nonlinear backlash is explicitly addressed by the simpler mode switching algorithm with less online calculation loads.

(C3). The active controller designed by the proposed method is tested via simulations based on a driveline dynamics model. The robustness is analyzed for various fluctuation patterns of driveline dynamics such as the plant parameters, the amount of backlash, and the driving conditions. Moreover, comparison studies with other traditional controllers such as a proportional-integral-differential (PID) controller tuned by the Ziegler-Nichols method are conducted in detail.

II. DRIVELINE DYNAMICS WITH NONLINEAR BACKLASH EFFECTS

A. DRIVELINE MODEL

Originating from our previous works [17], [39], Fig. 1(a) shows the driveline dynamical model that has been established as a simplification of an actual automobile driveline. This model is aimed at focusing on the transient oscillations due to an abrupt driving force change and nonlinear backlash.

TABLE 1. Parameters of drivetrain model.

Parameter	Value	Unit
M_B	0.232	kg
m_G	0.039	kg
M_E	1.04	kg
K_C	660.0	N/m
K_D	2.2×10^4	N/m
K_G	5.3×10^4	N/m
C_C	0.1	Ns/m
C_D	12.5	Ns/m
C_G	36.0	Ns/m
C_{cl}	1.5	Ns/m

The model parameters are listed in Table 1. The influence due to backlash is contained in the form of a discontinuous dead-zone region. More detailed explanations of this model can be founded in [17] and [40].

Fig. 1(b) represents the two modes of driveline dynamics. The contact mode allows for the coupling of the driven side M_E and the output side M_B (i.e., actuator and vehicle body).

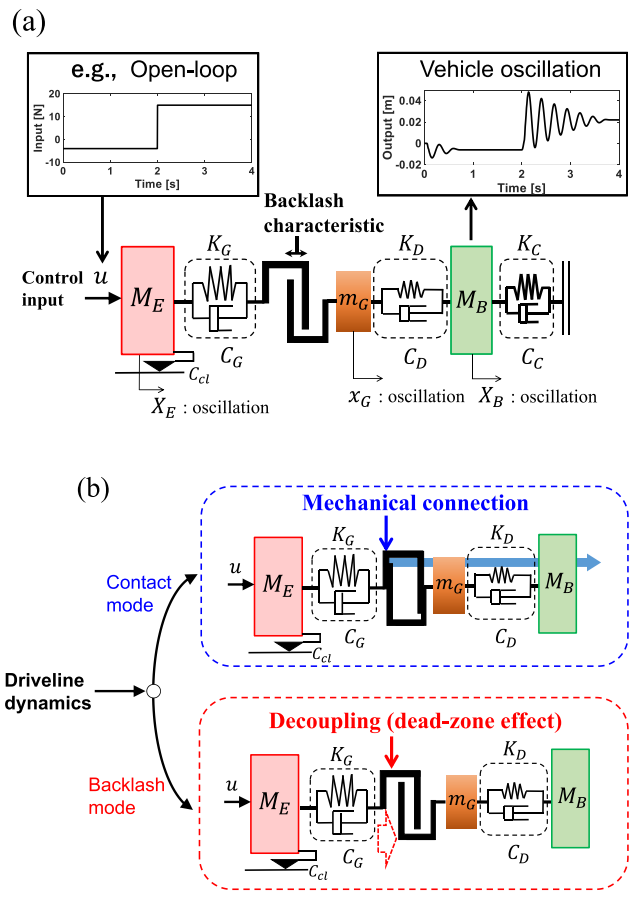

FIGURE 1. Driveline dynamics: (a) simplified model (b) contact and backlash modes.

In the backlash mode, they are forced to be decoupled because of clearance traversal.

B. MODELING FOR OSCILLATION CONTROL DESIGN

To design a baseline oscillation controller, the linearized model should be firstly derived from the driveline dynamics including nonlinearities such as the backlash. The previous studies have established the time-varying linear state equation of the plant model [17], [36]:

$$\dot{\boldsymbol{X}}_d = \boldsymbol{A}_d \boldsymbol{X}_d + \boldsymbol{B}_{d1} \boldsymbol{w}_d + \boldsymbol{B}_{d2} u \tag{1}$$

$$y_d = \boldsymbol{C}_d \boldsymbol{X}_d + \boldsymbol{D}_{d1} \boldsymbol{w}_d + D_{d2} u \tag{2}$$

Each coefficient matrix is given as (3), shown at the bottom of the next page.

$$\boldsymbol{X}_d = \begin{bmatrix} X_B & x_G & X_E & \dot{X}_B & \dot{x}_G & \dot{X}_E \end{bmatrix}^T \tag{4}$$

u is the control input, and $\boldsymbol{w}_d$ is the disturbance including force due to the backlash. The parameter Sw plays a role in expressing the dead-zone effect of backlash. Eq. (5) shows the switching rule [41], [42]. $|\delta|$ is the dead zone width and F is the force by the stiffness K_G. For deriving a baseline

controller, Sw is set to be 1.0.

$$\begin{aligned} F &= Sw \cdot K_G \cdot \Delta X + OKG \\ &= Sw \cdot K_G \cdot (X_E - x_G) + OKG \end{aligned}$$

$$Sw = \begin{cases} 1, & X_E - x_G > |\delta| \\ 1, & X_E - x_G < -|\delta| \\ 0, & |X_E - x_G| \le |\delta|, \end{cases}$$

$$OKG = \begin{cases} -|K_G \times |\delta||, & X_E - x_G > |\delta| \\ |K_G \times |\delta||, & X_E - x_G < -|\delta| \\ 0, & |X_E - x_G| \le |\delta| \end{cases} \quad (5)$$

The time-varying linear state equation of the plant model with the backlash and other nonlinear characteristics is also described in [17].

III. ACTIVE OSCILLATION SUPPRESSION WITH COMPENSATION FOR BACKLASH

The configuration of the proposed active control is demonstrated in Fig. 2. This system deals with both the contact mode and the backlash mode.

A. H_2 OUTPUT FEEDBACK VIBRATION CONTROLLER

To explicitly evaluate the transient responses of a vehicle body, the baseline controller is designed as an output feedback H_2 control [43], [44]. In the block diagram shown in Fig. 3(a) that is used to derive the controller, the H_2 norm $\|T_{zw}(s)\|_2^2$ of the transfer function $T_{zw}(s)$ from the external input w to the controlled variables $z = \begin{bmatrix} z_y & z_u \end{bmatrix}^T$ is minimized. The expanded plant $G(s)$, which includes the controlled object $P_c(s)$, a high pass filter $W_{Highpass}$, and a low pass filter $W_{Lowpass}$, is constructed to limit the effective controlled frequency band of the vehicle body vibration to a low-frequency band [17], [36]. The design is performed based on MATLAB's "Control System Toolbox" and "Robust Control Toolbox".

Q_i and R_i are important weighting constants that need to be tuned carefully. i indicates the number of iterations for the later offline optimization. z_y and z_u are amplifications of the vehicle vibration y_G and the control input u_G from the expanded plant by Q_i and R_i, respectively, as shown below:

$$z_y = \sqrt{Q_i} \cdot y_G \quad (6)$$

$$z_u = \sqrt{R_i} \cdot u_G \quad (7)$$

According to Eqs. (6) and (7), selection of Q_i and R_i affects the oscillation performance level. Similar discussions are also found in [31] and [36]. If more aggressive vibration suppressions are required, Q_i should be adjusted to a larger value. On the other hand, larger values of R_i give energy-saving control and put emphasis on robust stability. They have been manually and subjectively determined in our previous works [36].

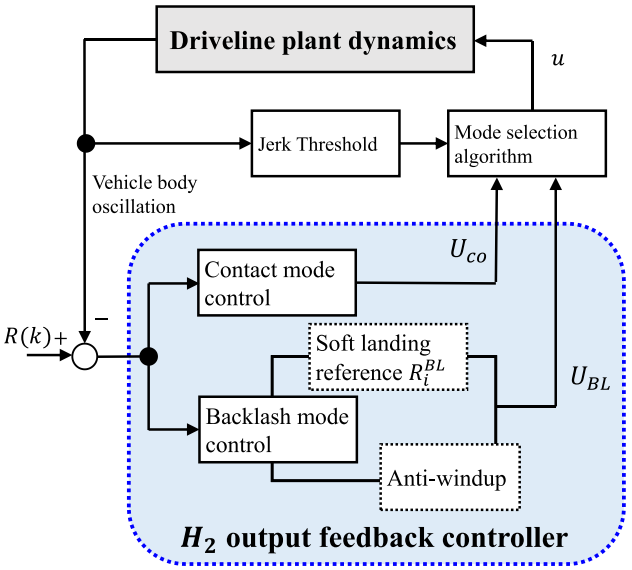

FIGURE 2. Active vibration suppression for contact mode and backlash mode.

$$A_d = \begin{bmatrix} 0 & 0 & 0 & 1 & 0 & 0 \\ 0 & 0 & 0 & 0 & 1 & 0 \\ 0 & 0 & 0 & 0 & 0 & 1 \\ -\frac{(K_D+K_C)}{M_B} & \frac{K_D}{M_B} & 0 & -\frac{(C_D+C_C)}{M_B} & \frac{C_D}{M_B} & 0 \\ \frac{K_D}{m_G} & -\frac{(SwK_G+K_D)}{m_G} & \frac{SwK_G}{m_G} & \frac{C_D}{m_G} & -\frac{(SwC_G+C_D)}{m_G} & \frac{SwC_G}{m_G} \\ 0 & \frac{SwK_G}{M_E} & -\frac{SwK_G}{M_E} & 0 & \frac{SwC_G}{M_E} & -\frac{(SwC_G+C_{cl})}{M_E} \end{bmatrix}$$

$$B_{d1} = \begin{bmatrix} 0 & 0 & 0 & 0 & \frac{1}{m_G} & -\frac{1}{M_E} \\ 0 & 0 & 0 & \frac{1}{M_B} & 0 & 0 \end{bmatrix}^T, \quad B_{d2} = \begin{bmatrix} 0 & 0 & 0 & 0 & 0 & \frac{1}{M_E} \end{bmatrix}^T, \quad C_d = \begin{bmatrix} 1 & 0 & 0 & 0 & 0 & 0 \end{bmatrix}$$

$$D_{d1} = 0, \quad D_{d2} = 0 \quad (3)$$

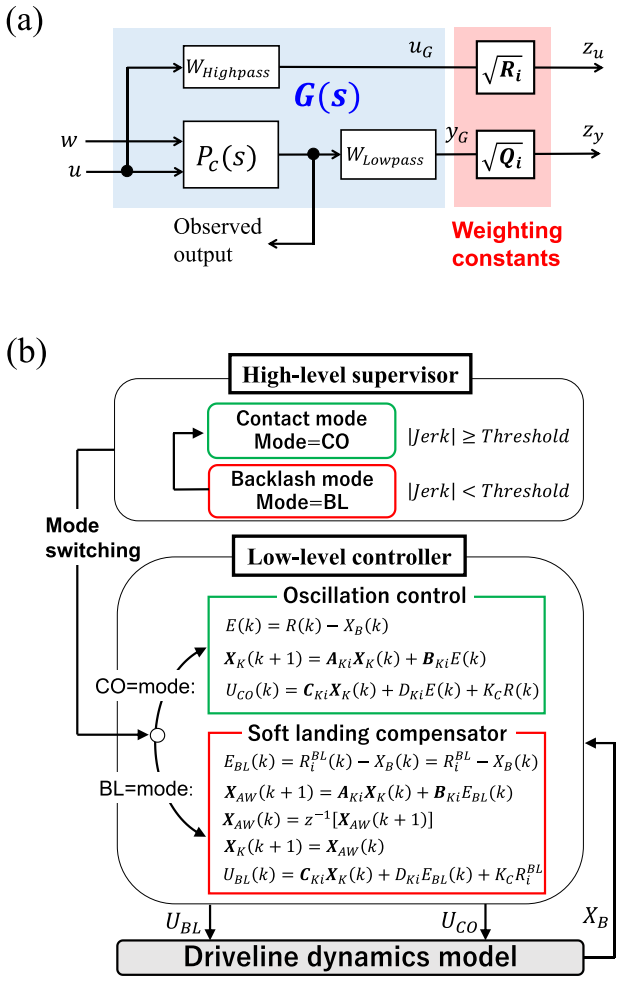

FIGURE 3. Active oscillation control system: (a) block diagram used to design a H_2 controller (b) mode switching algorithm.

B. MODE SWITCHING ALGORITHM TO ADDRESS NONLINEAR BACKLASH

To suppress the influences on the vehicle body due to backlash, the switching algorithm of the control modes shown in Fig. 3(b) is combined with the H_2 oscillation controller [17], [24]. The backlash mode control is aimed at allowing backlash to be quickly crossed from negative contact towards positive contact while alleviating the impact when the backlash crossing finishes via soft landing.

In the contact mode, the discretized state equation $(\boldsymbol{A}_{Ki}, \boldsymbol{B}_{Ki}, \boldsymbol{C}_{Ki}, D_{Ki})$ of the H_2 controller is normally performed as indicated in Eqs. (8)-(10).

In the backlash mode control indicated in Eqs. (11)-(15), the reference signal $R(k)$ commanded to the H_2 controller is switched to a key compensation reference R_i^{BL}. This value plays a role in making the controller generate a moderate control input to allow the backlash to be speedily traversed while making a soft landing when it finishes. Simultaneously, anti-windup, which temporarily stops updating the state vector $\boldsymbol{X}_K(k)$ of $(\boldsymbol{A}_{Ki}, \boldsymbol{B}_{Ki}, \boldsymbol{C}_{Ki}, D_{Ki})$, is applied to prevent the accumulation of the control errors induced by a dead-zone effect of the backlash. z^{-1} in Eq. (13) shows an one-control cycle delay operator to perform the anti-windup. Consequently, unnecessary large control inputs in the backlash mode are suppressed, helping the realization of a soft landing. More details on this compensation strategy are shown in [17] and [36].

Both the contact and backlash mode controls are performed based on the same single H_2 controller. Thanks to this simple structure, the design of multiple different controllers dedicated to handling the mode switching is unnecessary.

(Contact Mode Control):

$$E(k) = R(k) - X_B(k) \tag{8}$$
$$\boldsymbol{X}_K(k+1) = \boldsymbol{A}_{Ki}\boldsymbol{X}_K(k) + \boldsymbol{B}_{Ki}E(k) \tag{9}$$
$$U_{CO}(k) = \boldsymbol{C}_{Ki}\boldsymbol{X}_K(k) + D_{Ki}E(k) + K_C R(k) \tag{10}$$

(Backlash Mode Control):

$$E_{BL}(k) = R_i^{BL}(k) - X_B(k) = R_i^{BL} - X_B(k) \tag{11}$$
$$\boldsymbol{X}_{AW}(k+1) = \boldsymbol{A}_{Ki}\boldsymbol{X}_K(k) + \boldsymbol{B}_{Ki}E_{BL}(k) \tag{12}$$
$$\boldsymbol{X}_{AW}(k) = z^{-1}[\boldsymbol{X}_{AW}(k+1)]\,(\boldsymbol{X}_{AW}(k) = \boldsymbol{X}_K(k)) \tag{13}$$
$$\boldsymbol{X}_K(k+1) = \boldsymbol{X}_{AW}(k) \quad (\text{Substitute } \boldsymbol{X}_{AW}(k) \text{ for } \boldsymbol{X}_K(k+1)) \tag{14}$$
$$U_{BL}(k) = \boldsymbol{C}_{Ki}\boldsymbol{X}_K(k) + D_{Ki}E_{BL}(k) + K_C R_i^{BL} \tag{15}$$

For estimating the moment at which the backlash is finished to be crossed, a pulse-shaped steep value of a vehicle jerk, which originated from the time derivative of the vehicle acceleration discontinuously changed, is utilized. A threshold condition is established as below:

$$|Jerk(k)| \geq Threshold \tag{16}$$

Note that the soft-landing reference R_i^{BL} is key to the success of the above compensation. While overly large values of R_i^{BL} fail to make a soft landing, miniscule values of R_i^{BL} lead to deteriorated responsiveness. Finding a reasonable value for R_i^{BL} has been challenging and burdensome, imposing manual trial-and-error tasks on designers [17], [36].

IV. EFFICIENT TUNING SCHEME FOR ACTIVE OSCILLATION CONTROL CONSIDERING BACKLASH

A. SPSA

Focusing on its computational efficiency, the SPSA is used in the proposed tuning scheme. $L(\theta)$ is a positive scalar loss function to be minimized and $\theta \in \mathbb{R}^p$ is a design variable for $L(\theta)$. The θ update of the SPSA is shown in Eq. (17) [37]. The index i means the ith iteration. Here, $\hat{g}_i(\theta_i) \in \mathbb{R}^p$ is a stochastic estimate of $g(\theta) = \nabla L(\theta) = \partial L/\partial\theta$, the gradient of $L(\theta)$. $\Delta_i \in \mathbb{R}^p$ shows a random perturbation vector. $\hat{g}_{i,m}$ is the mth element of $\hat{g}_i$ and $\Delta_{i,m}$ is that of Δ_i. $\Delta_{i,m}$ is independent and symmetrically distributed about 0 with finite inverse moments $E[\left|\Delta_{i,m}^{-1}\right|]$ for all i, m [37], [38]. A Bernoulli

distribution is often employed as Δ_i [45].

$$\theta_{i+1} = \theta_i - a_i \hat{g}_i(\theta_i) \tag{17}$$

$$\hat{g}_{i,m}(\theta_i) = \frac{L(\theta_i + c_i\Delta_i) - L(\theta_i - c_i\Delta_i)}{2c_i\Delta_{i,m}} \tag{18}$$

$$\Delta_i = \begin{bmatrix} \Delta_{i,1} & \Delta_{i,2} & \cdots & \Delta_{i,p} \end{bmatrix}^T \tag{19}$$

The gains a_i and c_i are set to meet Eqs. (20)–(23) [37]. Equations (24) and (25) indicate typical selections of a_i and c_i [37], [38], where a, A, c, α, and γ show positive constants.

$$a_i > 0, \quad c_i > 0 \tag{20}$$

$$\lim_{i\to\infty} a_i \to 0, \quad \lim_{i\to\infty} c_i \to 0 \tag{21}$$

$$\sum_{i=1}^{\infty} a_i = \infty \tag{22}$$

$$\sum_{i=1}^{\infty} \frac{a_i^2}{c_i^2} < \infty \tag{23}$$

$$a_i = \frac{a}{(A+i)^\alpha} \tag{24}$$

$$c_i = \frac{c}{i^\gamma} \tag{25}$$

Table 2 compares some optimization techniques: Genetic algorithm (GA) [46], Particle swarm optimization (PSO) [47] and SPSA [37], [38], which are frequently applied to tune parameters of feedback control systems. This table summarizes the basic concepts and features of each algorithm [48] and contributes to highlight the difference of SPSA with respect to other optimization techniques.

Compared to other optimization techniques, a remarkable feature of SPSA is its superior computational efficiency. Equation (18) means that loss function calculations are necessary to be performed only twice to construct $\hat{g}_i$, and it is independent of the dimension p of the design variable θ_i [37]. Obtaining loss function values requires significant computational costs in practical optimization applications [49], [50]. Consequently, the SPSA, which requires few loss function computations at each iteration, is highly efficient, especially in multi-variable optimizations. The efficiency of SPSA has promoted its applications to various complicated engineering problems [50], [51], [52], [53], [54]. To the best of our knowledge, this research is the first example that SPSA is combined with an active oscillation controller for a driveline with backlash.

B. TUNING ALGORITHM BASED ON SPSA

The proposed tuning algorithm for the active driveline oscillation controller considering backlash is shown in Fig. 4.

Hereafter, the parameters updated by SPSA in Eq. (17) are called the design variables ($\theta_i \in \mathbb{R}^p$). Parameters for control system design are called tuning parameters. $J(\theta_i)$ indicates a positive scalar value loss function to measure the controller's attenuation performance. SPSA eventually outputs the θ_i value that minimizes $J(\theta_i)$. $C_{end} \in \mathbb{N}$ is the maximum number of iterations.

TABLE 2. Representative optimization algorithms.

Algorithm name	Basic concept	Features
Genetic Algorithm (GA) [46]	This is inspired by the principle of evolution in nature. The algorithm is based on modeling of the arrangement of genes and the regeneration process. The optimization proceeds with the operators such as natural selection, crossover, and mutation, and so on.	• Applicable to complicated problems. • Global search ability.
Particle Swarm Optimization (PSO) [47]	This is inspired by the social behavior of swarms, specifically mimicking the intelligence of birds flocking. Multiple particles search a solution by updating their position and velocity based on the best positions obtained so far.	• Robustness. • Global search ability. • Less operators and fewer parameters.
Simultaneous Perturbation Stochastic Approximation (SPSA) [37], [38]	The algorithm uses the stochastic approximation method for the gradient of a loss function to be minimized based on the simultaneous perturbation vector. Specifically, at each iteration, the gradient is stochastically estimated by providing simultaneous random perturbations for all design variables together.	• Easy to implement. • Presence of clear guideline to set parameters [45]. • Noise tolerance. • Higher computational efficiency regardless of the dimension of problems.

Algorithm. Optimized tuning of CO-mode and BL-mode controllers by SPSA

Initialize i
Initialize $\theta_0 \in \mathbb{R}^p \quad \forall m \in p$
for i = 1:1:C_{end} **do**
  Update $a_i \leftarrow a/((i+A)\hat{}\alpha)$;
  Update $c_i \leftarrow c/(i\hat{}\gamma)$;
  Generate perturbation vector Δ_i with Bernoulli distribution;
  Give perturbations to θ_i;
% Design active damping controllers for CO-mode and BL-mode
  Design $(\boldsymbol{A}_{Ki}, \boldsymbol{B}_{Ki}, \boldsymbol{C}_{Ki}, D_{Ki})$ and R_i^{BL} using $\theta_i + c_i\Delta_i$;
  Design $(\boldsymbol{A}_{Ki}, \boldsymbol{B}_{Ki}, \boldsymbol{C}_{Ki}, D_{Ki})$ and R_i^{BL} using $\theta_i - c_i\Delta_i$;
  Perform control simulation using controller based on $\theta_i + c_i\Delta_i$;
  Perform control simulation using controller based on $\theta_i - c_i\Delta_i$;
  Calculate $J(\theta_i \pm c_i\Delta_i)$;
  Calculate $\hat{g}_i$ using c_i, Δ_i, and $J(\theta_i \pm c_i\Delta_i)$;
  Update $\theta_i \leftarrow \theta_i - a_i\hat{g}_i$;
end for
Return θ_i

FIGURE 4. Pseudo code of the tuning algorithm based on SPSA.

The proposed method can automatically tune the oscillation controller, leading to a decrease in adjustments depending on the designer's trial-and-error tasks. The contact and backlash mode controls can be simultaneously optimized.

All the critical tuning parameters, Q_i, R_i, and R_i^{BL}, for the contact and backlash mode controls are stored in the vector θ_i. Equations (26)-(28) express Q_i, R_i, and R_i^{BL} by the design variable θ_i.

$$Q_i = |\theta_{i,1}| Q_0 \tag{26}$$
$$R_i = |\theta_{i,2}| R_0 \tag{27}$$
$$R_i^{BL} = |\theta_{i,3}| R_0^{BL} \tag{28}$$

$\theta_{i,m}$ shows the mth element of θ_i. Q_0, R_0, and R_0^{BL} are the initial values. θ_i is a three-dimensional vector. Those initial values were set as $Q_0 = 1.0$, $R_0 = 1.0$, and $R_0^{BL} = 1.0$.

Equation (29) shows the loss function $J(\theta_i)$ to be minimized as below:

$$J(\theta_i) = J_i = \frac{1}{N}\left\{ S_y \left(\sum_{k=1}^{N} \tilde{y}_{i,k}^2 \right) + S_u \left(\sum_{k=1}^{N} u_{i,k}^2 \right) \right\} \tag{29}$$

Here, $\tilde{y}_{i,k}$ shows the control error between the vehicle vibration and an ideal reference signal at the kth sampling point at the ith iteration. $u_{i,k}$ shows the control input at the kth sampling point at the ith iteration. N shows the number of sampling points. S_y and S_u show scaling factors on $\tilde{y}_{i,k}$ and $u_{i,k}$, respectively. This work sets those initial conditions as $S_y = 10^3$ and $S_u = 1$ by considering the scale difference between the first and second terms in Eq. (29). $J(\theta_i)$ is the sum of the mean square of the control error and that of the control input that originated from the active controller designed based on θ_i.

C. OPTIMIZATION SETTINGS

Table 3 indicates the settings for the SPSA shown in Eqs. (17)–(25). According to the guideline on the implementation of the SPSA [45], the settings in Table 3 can be determined.

TABLE 3. Setting for the SPSA employed in this study.

Properties	Value
Δ_i	Bernoulli ± 1 distribution with probability of 0.5 for each ± 1 outcome
a	1.0×10^{-5}
c	8.0×10^{-3}
A	1.0×10^{0}
α	0.602
γ	0.101
θ_0	$[1 \quad 1 \quad 1]^T$
Number of iterations	100

D. OPTIMIZATION RESULTS

Fig. 5 shows the tuning results given by the above approach. The iteration histories of each tuning parameter are shown in Figs. 5(a)-(c). Fig. 5(d) shows the iteration history of tuning of $J(\theta_i)$.

In Fig. 5(d), the initial value of $J(\theta_i)$, which is tremendously large, is finally decreased to a relatively small value

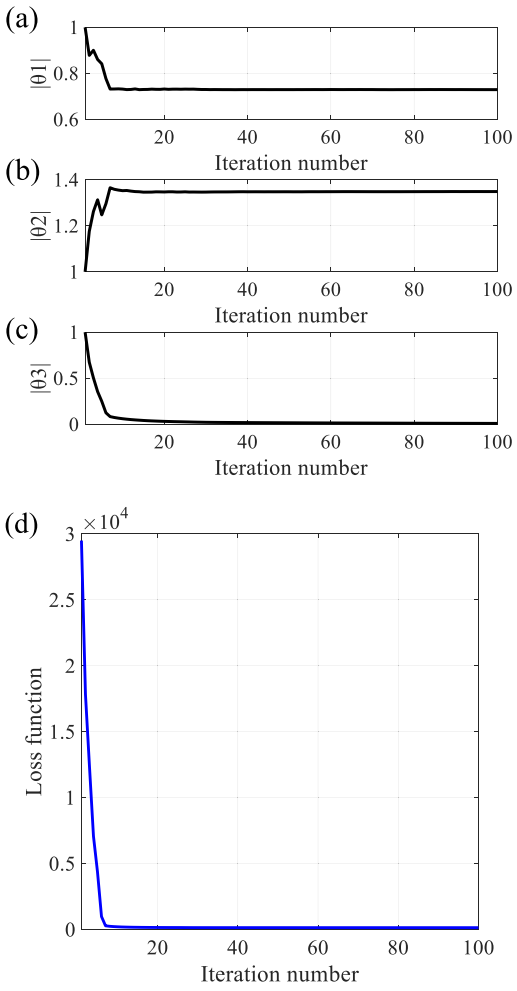

FIGURE 5. Tuning history: (a) Q_i (b) R_i (c) R_i^{BL} (d) loss function $J(\theta_i)$.

TABLE 4. Tuning result of the active oscillation control system (the mean of 5 trials).

Properties	Value
Q_{100}	0.7295
R_{100}	1.3487
R_{100}^{BL}	0.00931847
J_0	2.9482×10^4
J_{100}	122.3035

after the tuning process, meaning successful optimization of the active damping system. These tuning results are quantitatively summarized in Table 4. The large difference between the initial J_0 and tuned J_{100} values of the loss function is regarded as improved oscillation control performance.

V. SIMULATION VERIFICATIONS

A. SIMULATION CONDITIONS

The active oscillation controllers are validated via simulations with abrupt transient input changes.

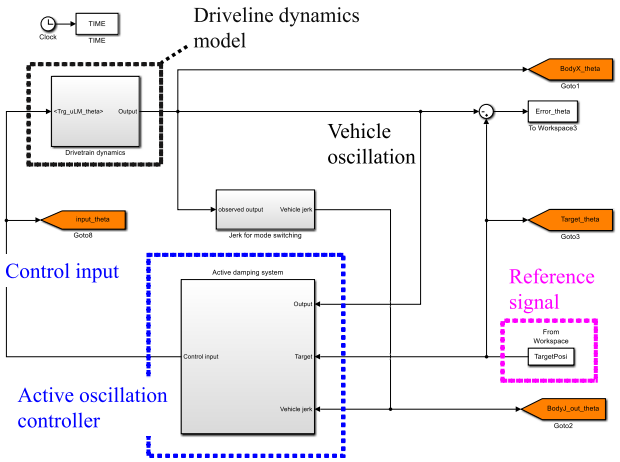

FIGURE 6. Simulink configuration used for simulation tests.

The verifications were performed based on MATLAB/Simulink. Fig. 6 indicates the configuration of the closed-loop system described by the Simulink diagram used for testing the proposed oscillation controller. The sampling time is set to be 2.0×10^{-5} s in all of the simulation tests.

The simulations involve some comparisons to other design approaches. One is an SPSA-based tuned H_2 controller without backlash compensation. Another is a control system shown in Fig. 2, but whose parameters were manually determined. In the latter one, we use an insufficiently adjusted value for R_i^{BL}.

B. SIMULATION RESULTS AND DISCUSSION

Fig. 7 shows the test result ("Case No. 0"). This case in Fig. 7 is defined as the simulation verification for the driveline system without any fluctuations in the model parameters: the verification for the nominal plant is called "Case No. 0" hereafter. The purpose of considering this condition is to firstly validate the basic damping performance owing to the proposed approach. The time responses of the vehicle oscillations and the control inputs are shown in the upper and lower graphs, respectively.

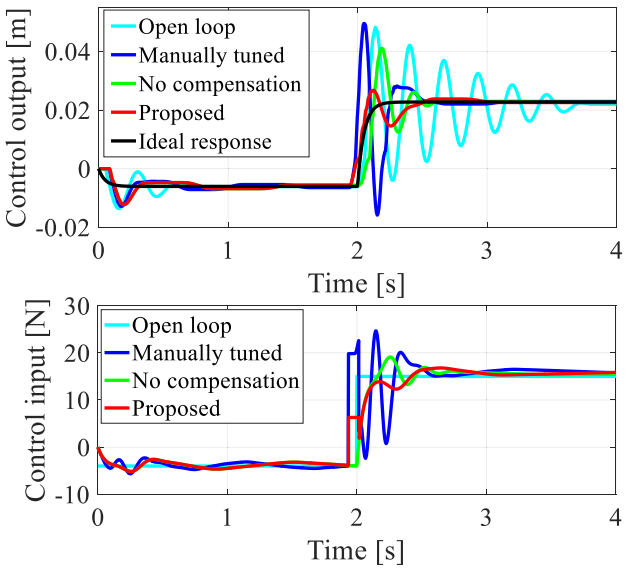

FIGURE 7. Time responses of the vehicle oscillation and the control input (Case No. 0).

As can be seen in Fig. 7, the good transient response performance is provided by the proposed method. Compared to the cyan (open loop response without controls), blue (insufficient manual tuning), and green (no compensations for backlash) lines, the vehicle oscillations after 2.0 s are sufficiently reduced in the red line (proposed method). We can see the importance of addressing backlash effects from the large overshoot indicated by the green line. Moreover, a comparison to the blue line tells us the necessity of proper control parameter tunings, especially for R_i^{BL}.

Table 5 lists the 2-norm of the control error between the ideal response (black line) and each oscillation to quantitatively compare the results shown in Fig. 7. Note that the proposed approach realizes the smallest value. This result illustrates the effectiveness of the SPSA-based tuning design.

TABLE 5. 2-norm computed for each oscillation response in fig. 7 (case No. 0).

Each control system	Value of 2-norm
Proposed method	0.9837
Insufficient manually tuned	3.0664
No compensation	1.6265
Open loop	3.2349

The 2-norm by the proposed method is decreased by 67.9203%, 39.5197%, and 69.5913% compared to "Insufficient manually tuned", "No compensation", and "Open loop", respectively.

The above control performance originates from the automatic controller tuning based on SPSA. The approach is aimed at reducing the designer's burden and costs due to trial-and-error-based manual tunings for designing driveline vibration controllers. This study focuses on automating the controller design process with an algorithm that is as simple and computationally efficient as possible. Therefore, SPSA was employed because it is the simple and efficient algorithm in terms of computational amount. Regarding the computational efficiency, SPSA is superior to other optimization algorithms, as described in section IV. This is because it has been theoretically shown that loss function calculations are necessary to be performed only twice at each iteration [37], [38], unlike other algorithms with a large number of the calculations.

In terms of the resultant control performance, however, comparative investigations with the application of other optimization techniques may need to be considered to pursue the

best vibration performance. This comparison will be included in our future works of this research.

C. TEST OF THE ROBUSTNESS AGAINST PLANT PARAMETER UNCERTAINTIES

This sub-section investigates the robustness of the controller against fluctuations in the plant parameters. Table 6 shows the two patterns of the specific fluctuations introduced in this research.

Figs. 8 and 9 show the simulation results with the plant parameter fluctuations "Case No. 1" and "Case No. 2", respectively. Specifically, these cases are defined as the verifications for the driveline dynamics with the fluctuations $\pm 10\%$ in each parameter and $\pm 30\%$ in the backlash, which are indicated in Table 6. Through simulations using such perturbed plant models, we aim to verify the robustness of the proposed control system.

TABLE 6. Fluctuation in plant model parameters.

Parameter	Fluctuation amount [%] (Case No. 1)	Fluctuation amount [%] (Case No. 2)
M_B	10	-10
m_G	-10	10
M_E	-10	-10
K_C	10	10
K_D	10	-10
K_G	-10	10
C_C	-10	10
C_D	10	-10
C_G	-10	10
C_{cl}	10	-10
Backlash length	30	-30

In both Figs. 8 and 9, the best damping performance is seen in the red line compared to the other lines. Even though the modeling errors in Table 6 are included in the plant model, the proposed method maintains good transient responses, implying its robustness. These results can be quantitatively evaluated by comparing the 2-norm values shown in Tables 7 and 8.

TABLE 7. 2-norm computed for each oscillation response in fig. 8 (case No. 1).

Each control system	Value of 2-norm
Proposed method	0.9489
Insufficient manually tuned	3.0128
No compensation	1.5506
Open loop	3.0877

The combination of the errors in backlash length and the other parameter fluctuations has serious effects on the degradation of the oscillations, as indicated by the blue and green lines. Considering what is different between the proposed method and the other controllers, we can conclude

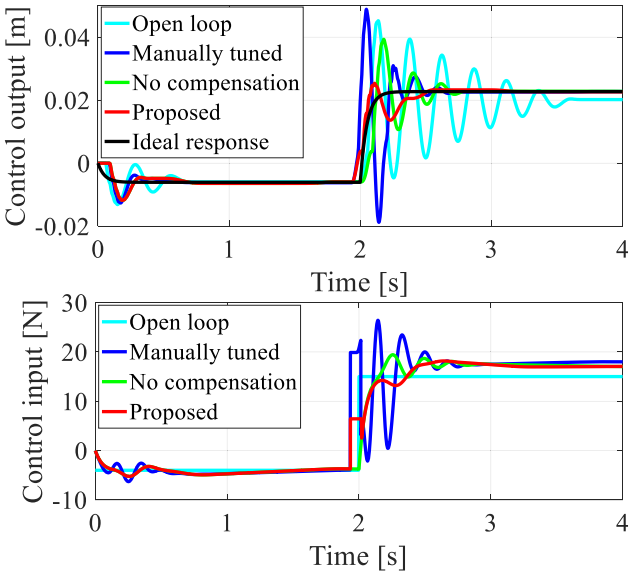

FIGURE 8. Simulation result with plant parameter fluctuations (Case No. 1).

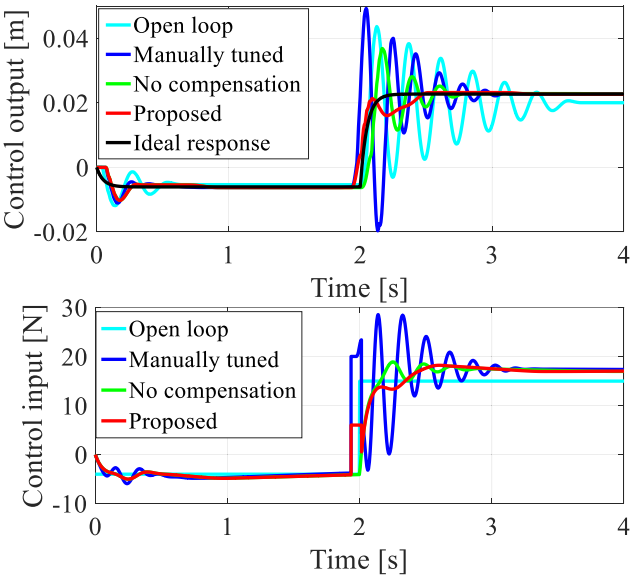

FIGURE 9. Simulation result with plant parameter fluctuations (Case No. 2).

TABLE 8. 2-norm computed for each oscillation response in fig. 9 (case No. 2).

Each control system	Value of 2-norm
Proposed method	0.8176
Insufficient manually tuned	3.4208
No compensation	1.3893
Open loop	2.9283

that the robustness is originating from the mode-switching-based compensation mechanism with the properly tuned parameters.

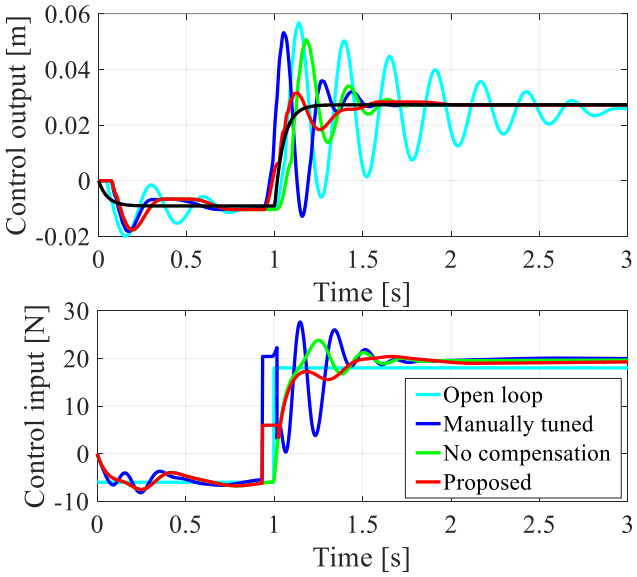

FIGURE 10. Simulation result with the changed driving condition (Case No. 3).

TABLE 9. 2-norm computed for each oscillation response in fig. 10 (case No. 3).

Each control system	Value of 2-norm
Proposed method	1.1793
Insufficient manually tuned	3.2699
No compensation	2.0728
Open loop	4.0804

D. TEST OF THE ROBUSTNESS AGAINST CHANGES OF DRIVING CONDITIONS

Fig. 10 shows another test result. This case is called "Case No. 3", which is defined as the verification when the driving condition is changed, unlike that in Fig. 7. Specifically, compared with that in Fig. 7, another ideal response (i.e., step reference signal) indicated by the black line that rises to a larger value is newly validated, and its rise time is also changed to 1.0 s. The purpose of considering Case No. 3 is to confirm the applicability of the proposed controller to different driving conditions.

Even though the driving condition (i.e., reference signal value) is changed, the red line demonstrates that the proposed method greatly suppresses the oscillations after 1.0 s, making the vehicle body response close to the reference signal (ideal response) shown by the black line. The comparison of the 2-norm values is given in Table 9. The larger value of "No compensation" than those in Tables 5, 7, and 8 can be translated into a more prominent influence of backlash increased by a greater driving condition. Therefore, it is considered that the robustness of the proposed method seen in Fig. 10 and Table 9 is provided by the SPSA-based optimized backlash compensation.

E. COMPARISON WITH TRADITIONAL TUNING METHOD

In order to further verify the proposed method's applicability to a driveline with nonlinear backlash, another traditional tuning approach is introduced just for comparison with the proposed approach. It is a PID oscillation controller tuned by the Ziegler-Nichols (Z-N) method, which is well-known to be effective [55]. This comparison test is called Case No. 4. That is, Case No. 4 is defined as the verification to compare the proposed SPSA-based active controller and the Z-N method-based PID controller. Firstly, the PID control is simply applied to a driveline without backlash to tune it via the Z-N method. After that, the proposed system and the PID controller are validated for the driveline with backlash to compare their oscillation suppressions. One of the purposes of investigating Case No. 4 is to further verify the effect of compensation for backlash due to the proposed method by comparing the absence of it (i.e., Z-N-based PID control). In addition, Case No. 4 is aimed at confirming the necessity of simultaneous optimizations for the contact and backlash mode controllers.

Unlike the proposed strategy in this study, the PID controller tuned by the Z-N method, which is a traditional approach, cannot include a backlash compensation (i.e., soft-landing compensator). It is because, in general, the Z-N method can tune only the PID controller applied to the contact mode of a driveline model without backlash. In other words, there is no tuning policy of the Z-N method for the case involving both the contact mode and the backlash mode. Hence, the Z-N method has no tuning guidelines to achieve the soft-landing purpose. Consequently, in this study, the PID controller was designed by applying the Z-N method for a driveline model without backlash (i.e., only the contact mode).

One of the main goals of this study is to clearly evaluate the compensation effect for backlash owing to the proposed vibration control system. This can be assessed by setting the presence or absence of a compensation mechanism for the control systems under consideration. In the comparative evaluation, a PID controller tuned by the Z-N method is suitable for comparison. This is because the Z-N method-based PID controller, although simple and practical, does not include compensation for backlash, as described above. Therefore, such a method to compare is appropriate to evaluate the difference between the proposed method, which can automatically tune backlash compensation and vibration control simultaneously, and other control methods. From another viewpoint, Z-N method-based tuned PID control is the most common approach, which is widely used in industry. Hence, it is suitable for comparison in terms of demonstrating the practicality of the proposed control method.

Fig. 11(a) shows the time response of the vehicle oscillation when the PID controller is applied to a driveline without backlash. Because the controlled plant (i.e., driveline) does not include nonlinear backlash, the yellow line shows that the PID controller designed by the Z-N method can achieve

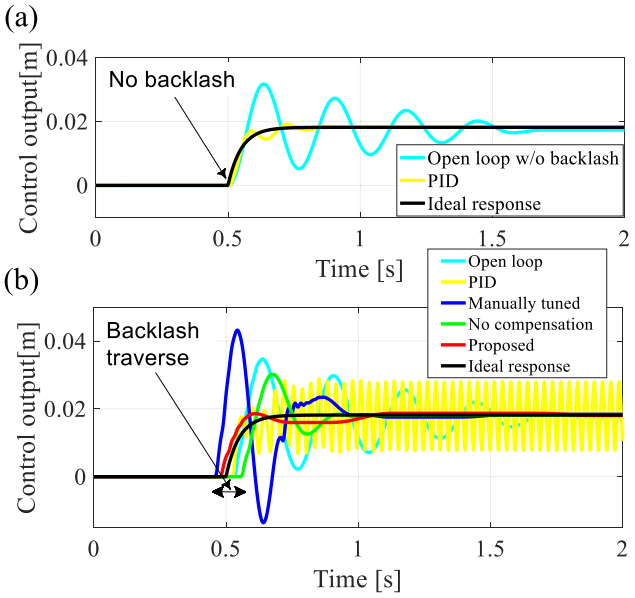

FIGURE 11. Control results of the vehicle oscillations: (a) the time response of the vehicle oscillation with application of the PID controller tuned by the Ziegler-Nichols method to a driveline without backlash (b) the time responses of the vehicle oscillation obtained by applying each control system to a driveline with nonlinear backlash (Case No. 4). The responses by the proposed method and the Z-N-based PID controller are shown in the red and yellow lines, respectively.

TABLE 10. 2-norm computed for each oscillation response in fig. 11 (case No. 4).

Each control system	Value of 2-norm
Proposed method	0.3974
Insufficient manually tuned	2.4863
No compensation	1.0042
PID control tuned by Z-N	2.8200
Open loop	1.8384

excellent oscillation control performance. The vehicle body response almost agrees with the ideal response indicated by the black line. In the yellow line in Fig. 11(a), which shows the control result for the driveline model without backlash, the PID controller has very little overshoot and no excessive gain. This means that the Z-N method is effective if the system does not include backlash.

However, such high control performance cannot be obtained by the above traditional PID controller when a driveline is subjected to the effects of nonlinear backlash. Fig. 11(b) shows the oscillation control result for the driveline with backlash. Each color line has the same meaning as that shown above. The oscillation shown by the yellow line is hardly reduced meaning that the same PID controller as that in Fig. 11(a) is no longer effective at all due to backlash, whereas the oscillation indicated by the red line is greatly reduced despite the presence of backlash.

The reason why the PID controller has the poor performance with large gain and overshoot in Fig. 11(b) is that it does not include any compensation mechanisms for backlash. Therefore, when just the PID controller is applied, the control errors are accumulated in the controller and the unnecessary (excessive) large control inputs are calculated due to the dead-zone effect of backlash, resulting in generation of the shock and intensive oscillation. On the other hand, the proposed approach has the backlash compensation, leading to the sufficient oscillation suppression indicated by the red line in Fig. 11(b). Consequently, the red line in Fig. 11(b) proves the applicability of the SPSA-based tuned active oscillation controller. The 2-norm value by each control method is also summarized in Table 10. The 2-norm by the proposed method is decreased by 84.0145%, 60.4236%, 85.9063%, and 78.3816% compared to "Insufficient manually tuned", "No compensation", "PID control tuned by Z-N", and "Open loop", respectively.

TABLE 11. Summary of decreasing (improvement) rates in 2-norm by the proposed method (cases No. 0 and No. 4).

Each control system for comparison	decreasing rate in 2-norm by the proposed method	
	Case No.0 (Fig. 7)	Case No. 4 (Fig. 11(b))
Insufficient manually tuned	67.9203%	84.0145%
No compensation	39.5197%	60.4236%
PID control tuned by Z-N	N/A	85.9063%
Open loop	69.5913%	78.3816%

For the representative verifications, which are Figs. 7 and 11(b), Table 11 summarizes the main results with the improvement rates by the proposed method. In Table 11, decreasing rates in 2-norm by the proposed method against other control systems are indicated.

The limitation of this research is the absence of experimental verifications as well as the necessity of the application to more realistic driveline models. These works will be included in our future research.

VI. CONCLUSION

With the aim at ensuring the comfortability and durability of a vehicle, this research presented the SPSA-based efficient tuning scheme of the active driveline oscillation controller considering backlash nonlinearity. The present methodology reduces low-resonant frequency oscillations induced in a driveline by the H_2 output feedback controller while mitigating the impact due to the nonlinearity of backlash by the simple control mode-switching-based compensation. The SPSA automatically searches for the optimal values of the tuning parameters required for the realization of the backlash compensation as well as the design of the H_2 controller. The resultant active control system was validated via several simulation tests that employ the nonlinear driveline oscillation model with backlash. Detailed comparative investigations with other traditional methods such as the PID controller tuned by the Ziegler-Nichols method were conducted. As a

result, the highest oscillation control performance by the proposed method was quantitatively observed, meaning the effectiveness of the SPSA-based tuning design.

The future tasks of this research include experimental verifications using an actual test device. Additionally, one of the future directions of this research will be dedicated to comparative investigations with the application of other optimization techniques.

REFERENCES

[1] A. G. A. Muthalif, K. A. M. Nor, A. N. Wahid, and A. Ali, "Optimization of piezoelectric sensor-actuator for plate vibration control using evolutionary computation: Modeling, simulation and experimentation," *IEEE Access*, vol. 9, pp. 100725–100734, 2021, doi: 10.1109/ACCESS.2021.3096972.

[2] C. Ahumada and P. Wheeler, "Reduction of torsional vibrations excited by electromechanical interactions in more electric systems," *IEEE Access*, vol. 9, pp. 95036–95045, 2021, doi: 10.1109/ACCESS.2021.3094172.

[3] J. Nie, Y. Yang, T. Jiang, and H. Zhang, "Passive skyhook suspension reduction for improvement of ride comfort in an off-road vehicle," *IEEE Access*, vol. 7, pp. 150710–150719, 2019, doi: 10.1109/ACCESS.2019.2946743.

[4] E. Atam, "Friction damper-based passive vibration control assessment for seismically-excited buildings through comparison with active control: A case study," *IEEE Access*, vol. 7, pp. 4664–4675, 2019, doi: 10.1109/ACCESS.2018.2886880.

[5] Y. S. Hamed, H. K. Alkhathami, and E. R. El-Zahar, "Utilizing nonlinear active vibration control to quench the nonlinear vibrations of helicopter blade flapping system," *IEEE Access*, vol. 8, pp. 203003–203016, 2020, doi: 10.1109/ACCESS.2020.3035611.

[6] Z. Hao, T. Wang, X. Cao, and Q. Zhang, "Design of eccentric mass-type vibration-damping electric actuator control system for non-fixed-wing aircraft," *IEEE Access*, vol. 8, pp. 219415–219429, 2020, doi: 10.1109/ACCESS.2020.3042854.

[7] Z. Jinyu, H. Song, J. Longyu, and Y. Fuyuan, "Active vibration control strategy for online application in a range extender," *IEEE Access*, vol. 11, pp. 26686–26702, 2023, doi: 10.1109/ACCESS.2023.3255418.

[8] A. Yonezawa, I. Kajiwara, and H. Yonezawa, "Novel sliding mode vibration controller with simple model-free design and compensation for actuator's uncertainty," *IEEE Access*, vol. 9, pp. 4351–4363, 2021, doi: 10.1109/ACCESS.2020.3047810.

[9] L. Chen, W. Shi, and Z. Chen, "Research on damping performance of dual mass flywheel based on vehicle transmission system modeling and multi-condition simulation," *IEEE Access*, vol. 8, pp. 28064–28077, 2020, doi: 10.1109/ACCESS.2019.2951618.

[10] Y. Hu, F. Yang, L. Du, J. Zhang, and M. Ouyang, "A novel method to actively damp the vibration of the hybrid powertrain by utilizing a flywheel integrated-starter-generator," *IEEE Access*, vol. 8, pp. 147045–147058, 2020, doi: 10.1109/ACCESS.2020.3014726.

[11] R. S. Vadamalu and C. Beidl, "Adaptive internal model-based harmonic control for active torsional vibration reduction," *IEEE Trans. Ind. Electron.*, vol. 67, no. 4, pp. 3024–3032, Apr. 2020, doi: 10.1109/TIE.2019.2908579.

[12] X. Chen, D. Peng, J. Hu, C. Li, S. Zheng, and W. Zhang, "Adaptive torsional vibration active control for hybrid electric powertrains during start-up based on model prediction," *Proc. Inst. Mech. Eng., D, J. Automobile Eng.*, vol. 236, Nov. 2021, Art. no. 095440702110561, doi: 10.1177/09544070211056176.

[13] Y. Yue, Y. Huang, D. Hao, and G. G. Zhu, "Model reference adaptive LQT control for anti-jerk utilizing tire-road interaction characteristics," *Proc. Inst. Mech. Eng., D, J. Automobile Eng.*, vol. 235, no. 6, pp. 1670–1684, May 2021, doi: 10.1177/0954407020973971.

[14] W. Li, W. Zhu, X. Zhu, Y. Xu, J. Yang, and Z. Li, "Torsional oscillations control of integrated motor-transmission system over controller area network," *IEEE Access*, vol. 8, pp. 4397–4407, 2020, doi: 10.1109/ACCESS.2019.2962828.

[15] W. Li, W. Zhu, X. Zhu, and J. Guo, "Robust oscillation suppression control of electrified powertrain system considering mechanical-electric-network effects," *IEEE Access*, vol. 8, pp. 56441–56451, 2020, doi: 10.1109/ACCESS.2020.2982317.

[16] P. Reddy, M. Shahbakhti, M. Ravichandran, and J. Doering, "Drivetrain clunk control via a reference governor," *IFAC-PapersOnLine*, vol. 54, no. 20, pp. 846–851, 2021, doi: 10.1016/j.ifacol.2021.11.277.

[17] H. Yonezawa, I. Kajiwara, S. Sato, C. Nishidome, M. Sakata, T. Hatano, and S. Hiramatsu, "Vibration control of automotive drive system with nonlinear gear backlash," *J. Dyn. Syst., Meas., Control*, vol. 141, no. 12, pp. 1–11, Dec. 2019, doi: 10.1115/1.4044614.

[18] P. Reddy, M. Shahbakhti, M. Ravichandran, and J. Doering, "Real-time predictive clunk control using a reference governor," *Control Eng. Pract.*, vol. 135, Jun. 2023, Art. no. 105489, doi: 10.1016/j.conengprac.2023.105489.

[19] P. Templin and B. Egardt, "A powertrain LQR-torque compensator with backlash handling," *Oil Gas Sci. Technol.-Revue d'IFP Energies nouvelles*, vol. 66, no. 4, pp. 645–654, Jul. 2011, doi: 10.2516/ogst/2011147.

[20] T. Pham, R. Seifried, A. Hock, and C. Scholz, "Nonlinear flatness-based control of driveline oscillations for a powertrain with backlash traversing," *IFAC-PapersOnLine*, vol. 49, no. 11, pp. 749–755, 2016, doi: 10.1016/j.ifacol.2016.08.109.

[21] H. Chu, W. Shi, Y. Jiang, and B. Gao, "Driveline oscillation damping for hybrid electric vehicles using extended-state-observer-based compensator," *Sustainability*, vol. 15, no. 10, p. 8143, May 2023, doi: 10.3390/su15108143.

[22] Z. Zhou and R. Guo, "A disturbance-observer-based feedforward-feedback control strategy for driveline launch oscillation of hybrid electric vehicles considering nonlinear backlash," *IEEE Trans. Veh. Technol.*, vol. 71, no. 4, pp. 3727–3736, Apr. 2022, doi: 10.1109/TVT.2022.3150009.

[23] Z. Zhou, R. Guo, and X. Liu, "A disturbance-compensation-based sliding mode control scheme on mode switching condition for hybrid electric vehicles considering nonlinear backlash and stiffness," *J. Vib. Control*, vol. 29, May 2022, Art. no. 107754632210961, doi: 10.1177/10775463221096195.

[24] C. Lv, J. Zhang, Y. Li, and Y. Yuan, "Mode-switching-based active control of a powertrain system with non-linear backlash and flexibility for an electric vehicle during regenerative deceleration," *Proc. Inst. Mech. Eng., D, J. Automobile Eng.*, vol. 229, no. 11, pp. 1429–1442, Sep. 2015, doi: 10.1177/0954407014563552.

[25] J. Zhang, B. Chai, and X. Lu, "Active oscillation control of electric vehicles with two-speed transmission considering nonlinear backlash," *Proc. Inst. Mech. Eng., K, J. Multi-Body Dyn.*, vol. 234, no. 1, pp. 116–133, Mar. 2020, doi: 10.1177/1464419319877332.

[26] R.-E. Precup, R.-C. David, E. M. Petriu, M.-B. Radac, and S. Preitl, "Adaptive GSA-based optimal tuning of PI controlled servo systems with reduced process parametric sensitivity, robust stability and controller robustness," *IEEE Trans. Cybern.*, vol. 44, no. 11, pp. 1997–2009, Nov. 2014, doi: 10.1109/TCYB.2014.2307257.

[27] S. Manna, G. Mani, S. Ghildiyal, A. A. Stonier, G. Peter, V. Ganji, and S. Murugesan, "Ant colony optimization tuned closed-loop optimal control intended for vehicle active suspension system," *IEEE Access*, vol. 10, pp. 53735–53745, 2022, doi: 10.1109/ACCESS.2022.3164522.

[28] C. J. Oglieve, M. Mohammadpour, and H. Rahnejat, "Optimisation of the vehicle transmission and the gear-shifting strategy for the minimum fuel consumption and the minimum nitrogen oxide emissions," *Proc. Inst. Mech. Eng., D, J. Automobile Eng.*, vol. 231, no. 7, pp. 883–899, Jun. 2017, doi: 10.1177/0954407017702985.

[29] J. J. Eckert, S. F. da Silva, F. M. Santiciolli, Á. C. de Carvalho, and F. G. Dedini, "Multi-speed gearbox design and shifting control optimization to minimize fuel consumption, exhaust emissions and drivetrain mechanical losses," *Mechanism Mach. Theory*, vol. 169, Mar. 2022, Art. no. 104644, doi: 10.1016/j.mechmachtheory.2021.104644.

[30] J. J. Eckert, T. P. Barbosa, F. L. Silva, V. R. Roso, L. C. A. Silva, and L. A. R. da Silva, "Optimum fuzzy logic controller applied to a hybrid hydraulic vehicle to minimize fuel consumption and emissions," *Expert Syst. Appl.*, vol. 207, Nov. 2022, Art. no. 117903, doi: 10.1016/j.eswa.2022.117903.

[31] C. Lin, S. Sun, P. Walker, and N. Zhang, "Off-line optimization based active control of torsional oscillation for electric vehicle drivetrain," *Appl. Sci.*, vol. 7, no. 12, p. 1261, Dec. 2017, doi: 10.3390/app7121261.

[32] E. Catenaro, S. Formentin, M. Corno, and S. M. Savaresi, "Auto-calibration with stability margins for active damping control in electric drivelines," in *Proc. Eur. Control Conf. (ECC)*, Jul. 2022, pp. 1186–1191, doi: 10.23919/ECC55457.2022.9838164.

[33] D. Song, J. Wu, D. Yang, H. Chen, and X. Zeng, "An active multiobjective real-time vibration control algorithm for parallel hybrid electric vehicle," *Proc. Inst. Mech. Eng., D, J. Automobile Eng.*, vol. 237, Oct. 2022, Art. no. 095440702211301, doi: 10.1177/09544070221130122.

[34] J. Wang, X. Hou, C. Du, H. Xu, and Q. Zhou, "A moment-of-inertia-driven engine start-up method based on adaptive model predictive control for hybrid electric vehicles with drivability optimization," *IEEE Access*, vol. 8, pp. 133063–133075, 2020, doi: 10.1109/ACCESS.2020.3010528.

[35] W. Wang, Y. Li, J. Shi, and C. Lin, "Vibration control method for an electric city bus driven by a dual motor coaxial series drive system based on model predictive control," *IEEE Access*, vol. 6, pp. 41188–41200, 2018, doi: 10.1109/ACCESS.2018.2859356.

[36] H. Yonezawa, I. Kajiwara, C. Nishidome, T. Hatano, M. Sakata, and S. Hiramatsu, "Active vibration control of automobile drivetrain with backlash considering time-varying long control period," *Proc. Inst. Mech. Eng., D, J. Automobile Eng.*, vol. 235, nos. 2–3, pp. 773–783, Feb. 2021, doi: 10.1177/0954407020949428.

[37] J. C. Spall, "Multivariate stochastic approximation using a simultaneous perturbation gradient approximation," *IEEE Trans. Autom. Control*, vol. 37, no. 3, pp. 332–341, Mar. 1992, doi: 10.1109/9.119632.

[38] J. C. Spall, "An overview of the simultaneous perturbation method for efficient optimization," *Johns Hopkins APL Tech. Dig.*, vol. 19, no. 4, pp. 482–492, 1998.

[39] H. Yonezawa, A. Yonezawa, T. Hatano, S. Hiramatsu, C. Nishidome, and I. Kajiwara, "Fuzzy-reasoning-based robust vibration controller for drivetrain mechanism with various control input updating timings," *Mechanism Mach. Theory*, vol. 175, Sep. 2022, Art. no. 104957, doi: 10.1016/j.mechmachtheory.2022.104957.

[40] H. Yonezawa, I. Kajiwara, C. Nishidome, S. Hiramatsu, M. Sakata, and T. Hatano, "Vibration control of automotive drive system with backlash considering control period constraint," *J. Adv. Mech. Des. Syst. Manuf.*, vol. 13, no. 1, pp. 1–16, 2019, doi: 10.1299/jamdsm.2019jamdsm0018.

[41] J. C. Gerdes and V. Kumar, "An impact model of mechanical backlash for control system analysis," in *Proc. Amer. Control Conf.*, vol. 5, 1995, pp. 3311–3315, doi: 10.1109/ACC.1995.532216.

[42] M. Nordin, J. Galic, and P.-O. Gutman, "New models for backlash and gear play," *Int. J. Adapt. Control Signal Process.*, vol. 11, no. 1, pp. 49–63, 1997.

[43] M. Chilali and P. Gahinet, "H_∞ design with pole placement constraints: An LMI approach," *IEEE Trans. Autom. Control*, vol. 41, no. 3, pp. 358–367, Mar. 1996, doi: 10.1109/9.486637.

[44] K. Zhou, J. C. Doyle, and K. Glover, *Robust and Optimal Control*. New Jersey, NJ, USA: Prentice-Hall, 1996.

[45] J. C. Spall, "Implementation of the simultaneous perturbation algorithm for stochastic optimization," *IEEE Trans. Aerosp. Electron. Syst.*, vol. 34, no. 3, pp. 817–823, Jul. 1998, doi: 10.1109/7.705889.

[46] J. H. Holland, "Genetic algorithms," *Sci. Amer.*, vol. 267, no. 1, pp. 66–73, 1992.

[47] J. Kennedy and R. Eberhart, "Particle swarm optimization," in *Proc. Int. Conf. Neural Netw.*, vol. vol. 4, 1995, pp. 1942–1948, doi: 10.1109/ICNN.1995.488968.

[48] S. Mirjalili, S. M. Mirjalili, and A. Lewis, "Grey wolf optimizer," *Adv. Eng. Softw.*, vol. 69, pp. 46–61, Mar. 2014, doi: 10.1016/j.advengsoft.2013.12.007.

[49] J. C. Spall, *Introduction to Stochastic Search and Optimization: Estimation, Simulation, and Control*, vol. 46, no. 3. Hoboken, NJ, USA: Wiley, 2003, doi: 10.1002/0471722138.

[50] A. Yonezawa, H. Yonezawa, and I. Kajiwara, "Parameter tuning technique for a model-free vibration control system based on a virtual controlled object," *Mech. Syst. Signal Process.*, vol. 165, Feb. 2022, Art. no. 108313, doi: 10.1016/j.ymssp.2021.108313.

[51] A. Yonezawa, H. Yonezawa, and I. Kajiwara, "Vibration control for various structures with time-varying properties via model-free adaptive controller based on virtual controlled object and SPSA," *Mech. Syst. Signal Process.*, vol. 170, May 2022, Art. no. 108801, doi: 10.1016/j.ymssp.2022.108801.

[52] M.-B. Radac, R.-E. Precup, E. M. Petriu, and S. Preitl, "Application of IFT and SPSA to servo system control," *IEEE Trans. Neural Netw.*, vol. 22, no. 12, pp. 2363–2375, Dec. 2011, doi: 10.1109/TNN.2011.2173804.

[53] S. Li, T. Wang, H. Ren, X. Kong, and X. Wang, "Coordination optimization of VSL strategy on urban expressway and main road intersection signal," *IEEE Access*, vol. 8, pp. 223976–223987, 2020, doi: 10.1109/ACCESS.2020.3044311.

[54] W. Yan, P.-L. Loh, C. Li, Y. Huang, and L. Yang, "Conquering the worst case of infections in networks," *IEEE Access*, vol. 8, pp. 2835–2846, 2020, doi: 10.1109/ACCESS.2019.2962197.

[55] H.-C. Yu, C.-S. Jang, and W.-Y. Peng, "Design methodology and self-turning velocity control for high-speed slim sensorless brushless direct current motors with self-lubricated bearings," *Mechanism Mach. Theory*, vol. 84, pp. 134–144, Feb. 2015, doi: 10.1016/j.mechmachtheory.2014.06.001.

HEISEI YONEZAWA (Member, IEEE) received the B.S., M.S., and Ph.D. degrees in engineering from Hokkaido University, Japan, in 2017, 2019, and 2021, respectively. Since 2021, he has been an Assistant Professor with the Graduate School of Engineering, Hokkaido University. His research interests include powertrain, vehicle systems, vibration control, robust control, and optimization. He received the Miura Prize for best students in the field of mechanical engineering from the Japan Society of Mechanical Engineers, in 2019.

ANSEI YONEZAWA (Member, IEEE) received the B.S., M.S., and Ph.D. degrees in engineering from Hokkaido University, Japan, in 2019, 2021, and 2023, respectively. Since 2023, he has been a specially appointed Assistant Professor with the Graduate School of Engineering, Hokkaido University. His research interests include active vibration control, robust control, stochastic optimization, fractional-order control, and data-driven control. He received the Hatakeyama Prize and the Miura Prize given for best students in the field of mechanical engineering from the Japan Society of Mechanical Engineers, in 2019 and 2021, respectively.

ITSURO KAJIWARA received the B.S. degree in engineering from Tokyo Metropolitan University, in 1986, and the M.S. and Ph.D. degrees in engineering from the Tokyo Institute of Technology, in 1988 and 1993, respectively. From 1990 to 2000, he was an Assistant Professor with the School of Engineering, Tokyo Institute of Technology, where he was an Associate Professor with the Graduate School of Engineering, from 2000 to 2008. Since 2009, he has been a Professor with the Graduate School of Engineering, Hokkaido University. His research interests include vibration, control, structural health monitoring, and laser application.